JOURNAL OF GEOPHYSICAL RESEARCH, VOL. 92, NO. C3, PAGES 2883–2900, MARCH 15, 1987

Turbidity Currents and Submarine Channel Formation in Rupert Inlet, British Columbia 2. The Roles of Continuous and Surge-Type Flow

ALEX E. HAY

Department of Physics and Newfoundland Institute for Cold Ocean Science, Memorial University of Newfoundland St. John's, Newfoundland, Canada

Acoustic backscatter images are presented of the continuous flow turbidity current resulting from mine tailing discharge into Rupert Inlet. The current flows partially within a submarine channel, which both hooks to the left and meanders. The images show the turbidity current spilling over the outer levees at channel bends. A model for continuous turbidity flow incorporating overspill is developed and applied to the left-hooking section of the submarine channel. It is very likely that the observed overspill is primarily an inertial effect resulting from the outer bank being more sharply curved than the channel axis. The model results are combined with a sediment accumulation budget based on successive seismic profiling surveys and with results for surge-type flows (taken from the companion paper (Hay, this issue)). It shows that surges are primarily responsible for the transport of tailing to large distances from the point of discharge and should recur at 1- to 2-day intervals on average. This is consistent with the characteristics of coarse-grained turbidites observed in cores from the levees. Relative to the intervening fine-grained mud deposits the turbidites increase both in thickness and frequency in the downchannel direction. Furthermore, the surge recurrence interval obtained from the number of turbidites per core and the local accumulation rate is 2–5 days, essentially the same as that obtained from the model. Suspended tailing transport within the channel appears to be dominated by surge-type turbidity currents except close to the outfall. It is concluded that the surge-type flows are most responsible for the formation and morphology of much of the channel. It is not clear, however, that the meanders are formed principally by surges. Although the surges occur frequently and transport most of the sediment in the meander reach, the volume transport is dominated by continuous flow.

1. INTRODUCTION

Turbidity currents represent one of the primary mechanisms by which terrigenous sediments have, over time, been transported into the deep ocean. They have long been held responsible for the formation of the submarine canyon, channel, and fan systems which start at the edge of the continental shelf and extend seaward over the abyssal plains. Our knowledge of this process comes principally from the extensive geological literature on turbidites and laboratory experiments with gravity currents, rather than direct observations of turbidity currents themselves and their effects on submarine channel morphology.

The absence of instances in which turbidity currents, particularly surge-type flows, has been observed in developing subaqueous channels makes the problem of relating channel morphology to turbidity current properties rather difficult. There are many reasons for wanting to establish such relationships, not the least of which is the contribution that would be made to our understanding of the development of deep-sea fan deposits. Several studies have obtained promising results by inferring the properties of turbidity currents from submarine channel morphology alone (see the review by *Komar* [1977]) or from morphology combined with the distribution of turbidite deposits [*Bowen et al.*, 1984]. These studies illustrate both the potential of the approach and the limitations imposed by observations made only after the fact.

The Rupert Inlet study provides a case history of submarine channel development including observations of both surge-type and continuous flow turbidity currents and identification of turbidites in the sediments. The channel itself exhibited many features found in deep-ocean submarine channels: left-hooking and levee asymmetry [*Menard*, 1955; *Komar*, 1969], meanders [*Damuth et al.*, 1983; *Bellaiche et al.*, 1986], and a downstream decrease in channel relief and width [e.g., *Bellaiche et al.*, 1986]. Interpretation of the development of these features in the Rupert Inlet system requires that the effects of surge-type flows be separated from those of the continuous turbidity current associated with the discharge. The purpose of this article is to make this separation.

The first studies of turbidity currents and channel development in mine tailing disposal systems appear to have been made by *Carstens and Tesaker* [1972] and also *Tesaker* [1975] and *Normark and Dickson* [1976*a*, *b*]. In both studies, direct current measurements were obtained in continuous flow turbidity currents in the vicinity of mine tailing outfalls, and channelization of the deposit was found.

The paper begins with a brief description of methods in section 2. Section 3 provides the necessary background data on the submarine channel and the tailing deposit in Rupert Inlet. The acoustic observations of the continuous flow turbidity current are presented in section 4. Section 5 is an analytic treatment of continuous flow including overspill. The limitations of this model and the problem of maintaining a quasi-steady equilibrium morphology through a combination of deposition from continuous flow and removal by slump-generated surges are examined in section 6.

2. EXPERIMENTAL METHODS

Ross Laboratories model 200 acoustic sounders operating at a 0.1-ms pulse length were used in these experiments. Position fixes were made using a microwave positioning system,

Paper number 6C0655.
0148-0227/87/006C-0655$05.00

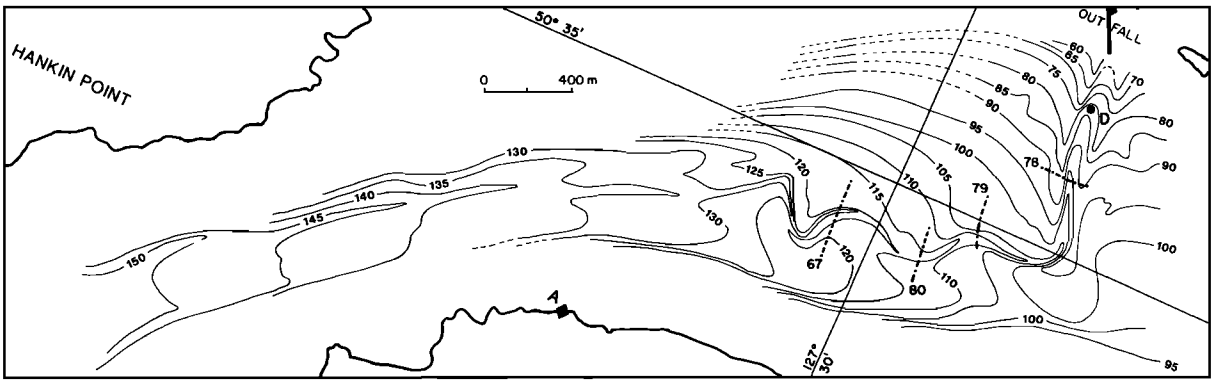

Fig. 1. Tailing deposit bathymetry in November 1976 during the meandering channel phase. Contours in meters. The dashed lines are acoustic sounding lines 78, 79, 80, and 67 (see text).

unless otherwise indicated. The continuous seismic profiling data were collected using a boomer and a linear hydrophone array. Total suspended particulate concentrations were determined gravimetrically after vacuum filtration of the sample through a 0.4-μm nominal pore size Nuclepore filter [*Hay*, 1981, 1983]. Some values of suspended particulate concentration are reported here which were determined using 0.45-μm nominal pore size Millipore filters and pressure filtration. The filters were weighed in the petrie dish in which each was stored. Material on the dish resulting from handling would therefore cause errors. However, because the measured concentrations are large (about 0.25 kg m^{-3}) and the volume filtered was 1.2 L, by far the largest change in weight is due to the suspended particulate on the filter, so these errors are not believed to be important.

3. Background

3.1. *Channel Characteristics*

The bathymetry of the mine tailing deposit in Rupert Inlet in November 1976 is shown in Figure 1. The tailing is discharged from the 1.1-m diameter outfall at an approximate rate of 380 kg s^{-1} at a depth of 49 m in the form of a slurry of 10% solids, 40% freshwater, and 50% seawater, by volume. The tailing particles are typically 65–75% smaller than 0.074-mm diameter, with a nominal median diameter of 0.030 mm.

The submarine channel in Figure 1 is in its so-called meandering channel phase. From the start of the channel near the outfall the "upper reach" extends cross inlet, hooking slightly to the left (in the downchannel sense) and then enters the "meander reach," which is located in the central trough of the inlet. The straight "lower reach" is below the meander reach.

The channel depth is plotted as a function of axial distance in Figure 2*a*. The axial slope of the upper reach is between 9.5° and 12° at the top, decreasing to 1.9° at the bottom, while the slopes of the meander and lower reaches are 0.91° and 0.47°, respectively. The channel relief and width are shown in Figures 2*b* and 2*c*. The relief is defined as the vertical distance from the channel bottom to the crest of the higher of the two levees. The width is the full width: the horizontal distance between levee crests, corrected for the angle between the sounding line and the channel talweg. In the meander reach the channel width was difficult to determine unambiguously because of the absence of a well-defined inner levee. This accounts for the smaller density of points in this section of the diagram and means that the uncertainty of the widths given for this reach is much larger than for the upper and lower reaches. The channel relief and width both undergo a pronounced increase in the 200-m section of the upper reach near the outfall. There is another sharp increase in relief at the bottom of the upper reach, which corresponds to the height above channel bottom of the levee on the southeast side of the first bend. Both relief and width exhibit overall decreases downchannel from this area.

Consider the upper reach. The top 200- to 300-m section of this reach is steep (axial slope, 9.5°–12°), while the axial slope in the remaining 700- to 800-m-long section is much less (2.2°) and relatively constant (Figure 2*a*). The channel cross-sectional area may be taken to be proportional to the product of relief and width. This quantity increases with distance away from the outfall in the top 200-m-long section but decreases with axial distance throughout much of the rest of this reach (Figures 2*b* and 2*c*). A pronounced increase in cross section is found at the base of the upper reach at the first bend. The channel cross section then decreases on average throughout the rest of the channel.

3.2. *Sediment Budget*

Continuous seismic profiling surveys were conducted annually after commencement of mining operations in 1971 until 1975, and again in 1977. The submarine channel was first recognizable as a pronounced feature in the 1974 survey which, together with the results of the two subsequent surveys, is presented in Figure 3. These data are discussed in more detail by *Hay et al.* [1983*a*]. The deposit thickness information in Figure 3 can be used to compute a sediment budget for the basin, which will provide estimates of the net sediment transport from one part of the basin to another. This requires, however, that the deposited tailing be distinguished from material derived from the waste dump, which is shown on the north flank of the inlet in Figure 3.

The waste dump material is low-grade rock which is bulldozed into the inlet at a rate about 3–4 times the rate of tailing discharge. The material spans a broad size range, from boulders to clay-sized particles. The fine waste dump material is physically indistinguishable from tailing, and it must be assumed that this material can be carried considerable distances from the dump. Equally, tailing must be deposited in the vicinity of the waste dump. It was therefore assumed that each source contributed equally to the volume of material on

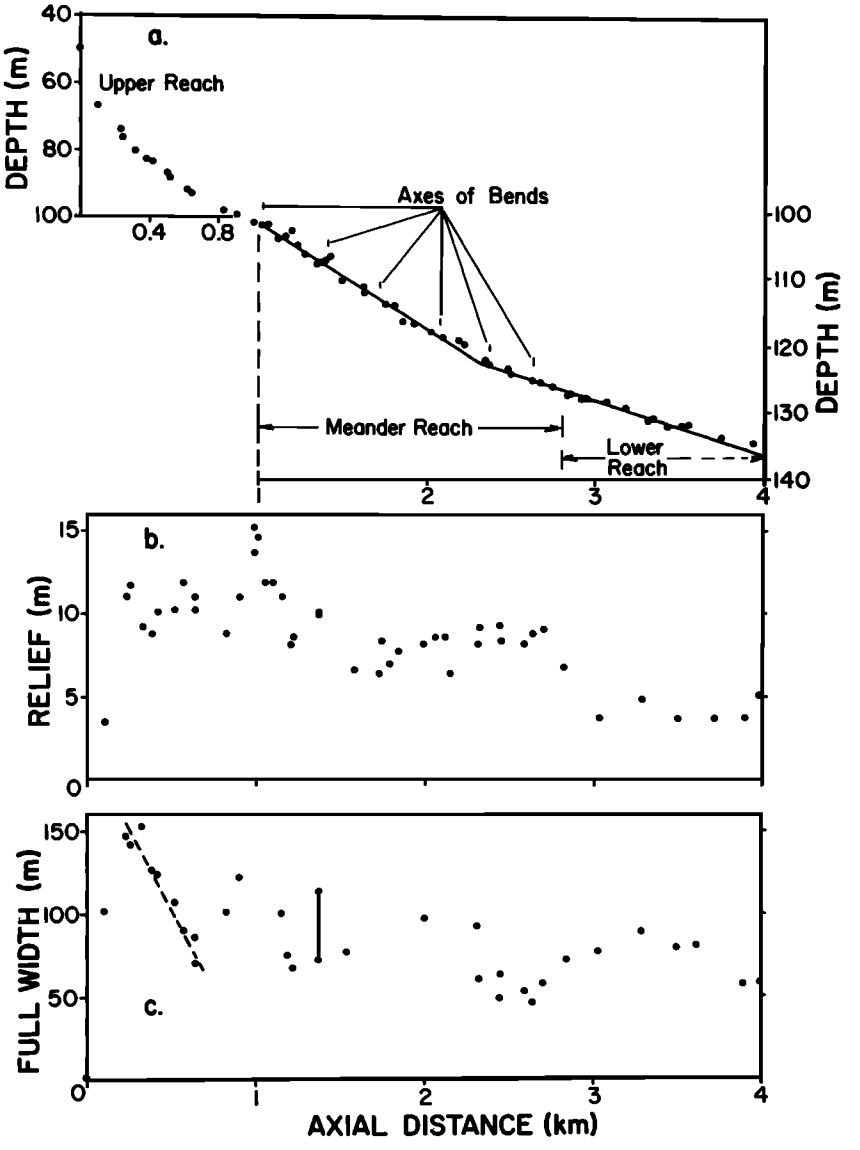

Fig. 2. Axial profiles of (*a*) channel depth, (*b*) channel relief, and (*c*) channel width for the November 1976 survey (Figure 1) during the meandering channel phase. The dashed line in Figure 2*c* emphasizes the linear decrease in channel width in the lower part of the upper reach; the solid vertical line at 1.4 km illustrates the range of width estimates which can be inferred from the same sounding line in the meander reach depending on one's choice for the crest of the inner levee.

either side of the saddle point between the two deposits, which is shown by the line XX′ in Figure 3.

The volume of the tailing deposit was determined by integrating the area enclosed by each of the thickness contours in Figure 3 using a planimeter. Assuming a dry bulk density of 1.3 g cm^{-3} for the tailing [*Hay and Waters*, 1985], the mass of the tailing deposit was computed and compared to the total reported discharge. The results are given in Table 1. The computed values are quite sensitive to the value of the dry bulk density and, to a lesser extent, to the unknown speed of sound in the deposit (1500 m s^{-1} was assumed). Since both parameters vary with deposit thickness due to compaction, the assumption of constant values is not strictly valid. Furthermore, the continuous seismic profiler is insensitive to tailing deposits much less than 1.5 m thick because of ringing in the outgoing pulse. The volume of this material was estimated by extrapolating the area versus thickness curves to zero thickness. Nevertheless, good agreement (within 10%) exists between the values for the total tailing deposited and the total tailing discharged. We conclude that the tailing and waste dump deposits are separated reasonably well by the line XX′.

The tailing deposit was divided into proximal and distal zones by the line YY′ below the meander reach (Figure 3). The volume of the deposit was determined for the proximal zone in the same manner as described above. The equivalent mass accumulation rate was quite consistent for the two periods, 148 and 140 kg s^{-1}, leaving an average of 240 kg s^{-1} of material to be transported out of the proximal zone. Continuous and surge-type turbidity currents, and the inlet circulation, contribute to this transport.

3.3. *Channel Pattern Persistence*

Detailed surveys of the meandering channel were conducted in November 1976 (Figure 1) and January 1977 (Figure 3*c*). In addition, a side scan survey was conducted in June 1977 (not shown). Essentially the same channel pattern as that in Figure

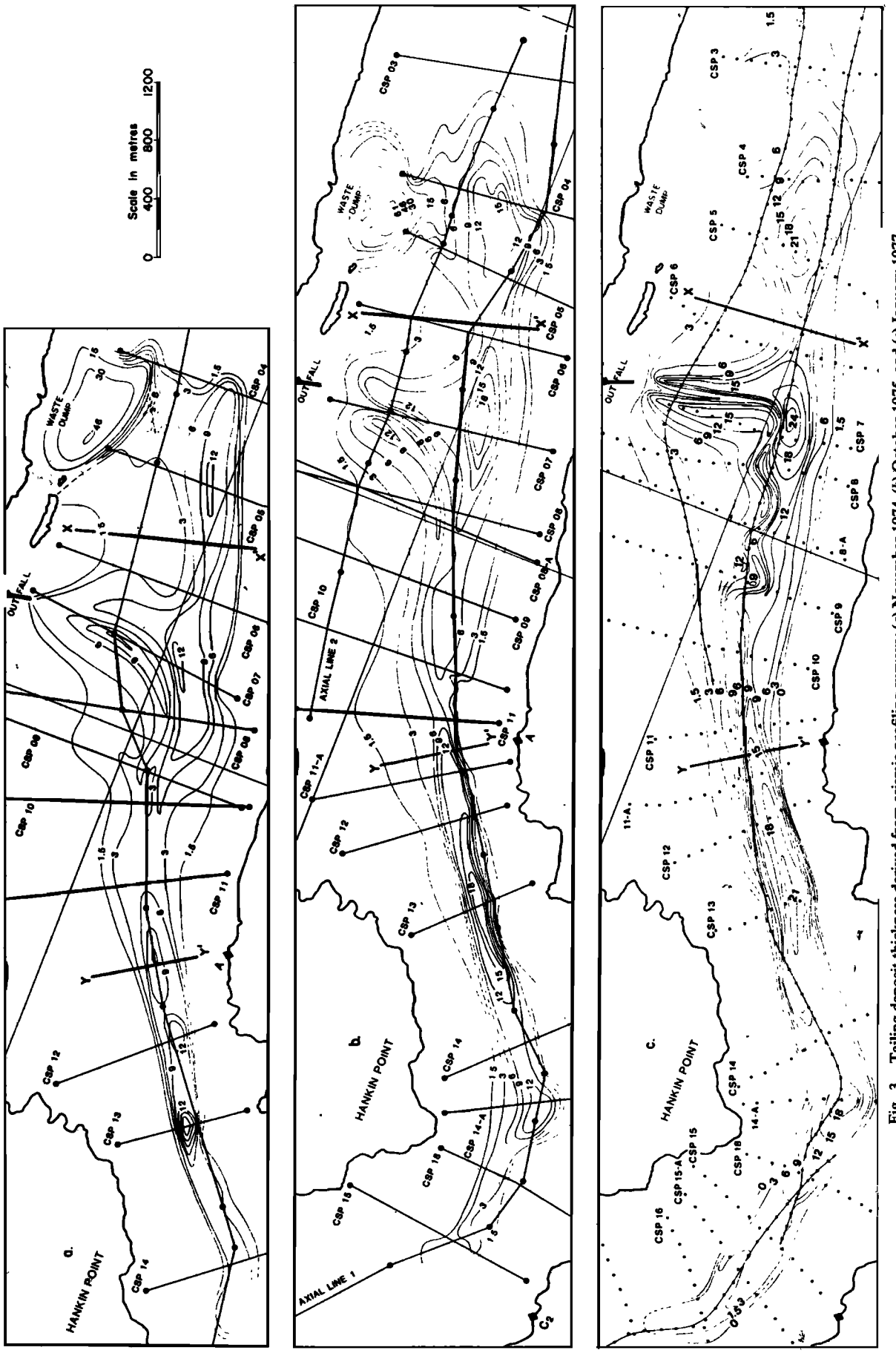

Fig. 3. Tailing deposit thickness derived from seismic profiling surveys: (*a*) November 1974, (*b*) October 1975, and (*c*) January 1977.

TABLE 1. Volume of Tailing Deposit From Seismic Profiling Surveys: Computed (See Text) and Reported Average Rates of Tailing Discharge Between Surveys

Survey Date	Volume, $\times 10^5$ m^3	Computed Rate, kg s^{-1}	Reported Rate, kg s^{-1}
Nov. 29, 1974	12.58		
		385	420
Oct. 21, 1975	15.64		
		348	352
Jan. 12, 1977	19.82		

1 persisted throughout this 7-month interval [*Hay et al.*, 1983*a*]. Additional surveys with less accurate navigation show that the channel was present for a period of about 3 years [*Hay et al.*, 1983*a*]. It is not known whether the meanders persisted that long. It is known from turbidites found in cores, however, that surge-type turbidity currents occurred at 1- to 5-day intervals [*Hay et al.*, 1983*b*]. Using the 7-month interval as the minimum time scale of channel pattern change, it is clear that for a large number of sequential surges, the channel was essentially the same. The submarine channel in Figure 1 is therefore taken to be in a slowly changing, or quasi-steady, state of equilibrium with the continuous flow and surge-type turbidity currents responsible for its formation.

4. Continuous Flow Observations

An acoustic image of the discharge plume in the upper reach is shown in Figure 4. The line location is shown in Figure 1. The channel appears as if viewed looking downstream, that is, with the higher west levee on the right. The bottom echo is the thin dark line immediately above the band of uniform light gray (a product of the "Fineline" feature in the receiver). Large amplitude scatterers, probably fish, are distributed throughout the displayed section of the water column. The backscattered signal from the discharge plume is concentrated on the right-hand side of the channel and can be seen spilling out of the channel beyond the crest of the higher west levee. Side echo from the bank partially masks the plume within the channel on the right-hand side. This profile is typical of those acquired in this portion of the upper reach. The others have been discussed by *Hay* [1981]. All exhibit the same tendency on the part of the plume to hug the right bank and spill over the right levee, independent of the phase of the tide.

Figure 5 is a series of three profiles showing the channelized plume at successively increasing distances from the outfall in the meander reach. Again, the channel appears as if viewed looking downstream, and the line locations are shown in Figure 1. These profiles all show the plume spilling over the levee of the outer bank in a bend. The point farthest downchannel at which the plume was detected in November 1976 was line 67 (Figure 5*c*). The receiver gain was lower for this profile than it was for the others, which is why the plume is only barely discernable over the right bank and levee.

Profiles of total suspended particulate near the outfall at station D (Figure 1) are shown in Figure 6. These samples were collected while the vessel was moored fore-and-aft over the channel. The zone of high concentration begins at about 6–10 m above bottom, consistent with the acoustic image in Figure 4. Near-bottom concentrations ranged from 0.03 to 0.37 kg m^{-3}, and although samples closer than 3 m to the bottom were not obtained, a reasonable mean value in the 8-m-thick layer next to the bottom is 0.25 kg m^{-3}.

5. Theory: Continuous Turbidity Flow in the Upper Reach

A theoretical model is needed to provide estimates of tailing transport and deposition due to channelized continuous flow. Because the effects of both channel curvature and overspill must be included, previous formulations are unlikely to be suitable. These either do not incorporate overspill [*Komar*, 1969] or invoke a special type of overspill (e.g., flow stripping [*Bowen et al.*, 1984]).

The present model is developed for the upper reach, for which we have information on sediment input, suspended sediment concentration, and the cross-channel slope of the interfacial region between the continuous flow turbidity current

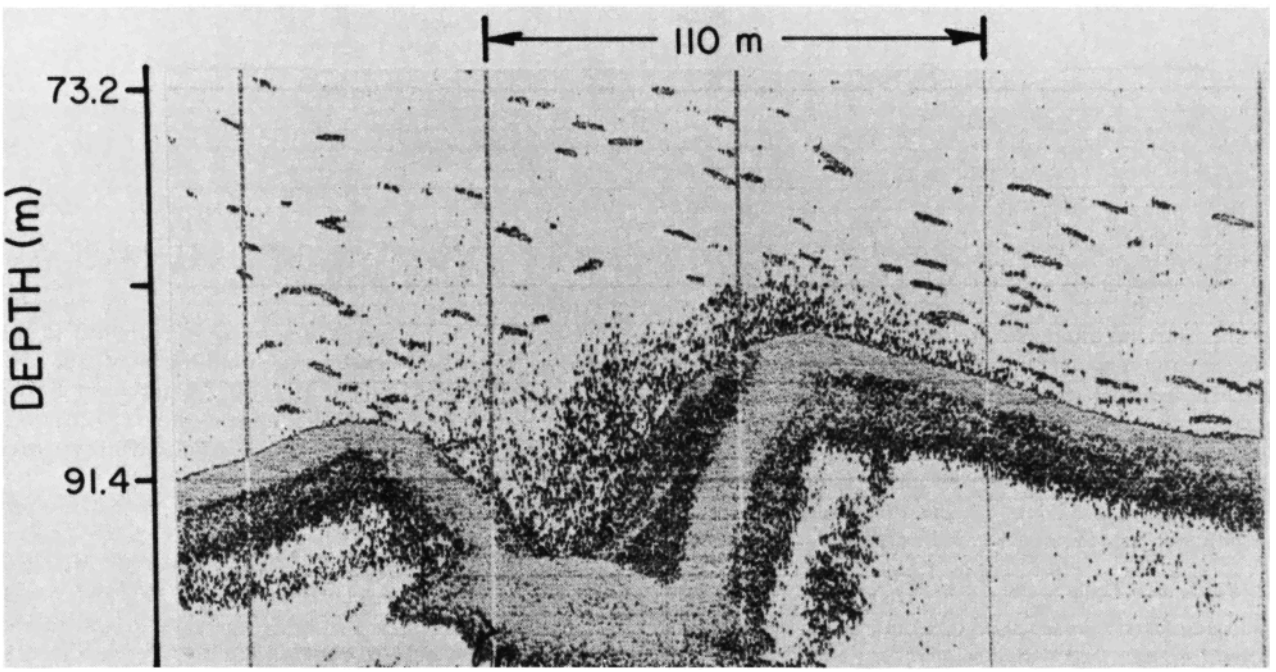

Fig. 4. The 200-kHz acoustic image of the channelized discharge plume along line 78. See Figure 1 for line location.

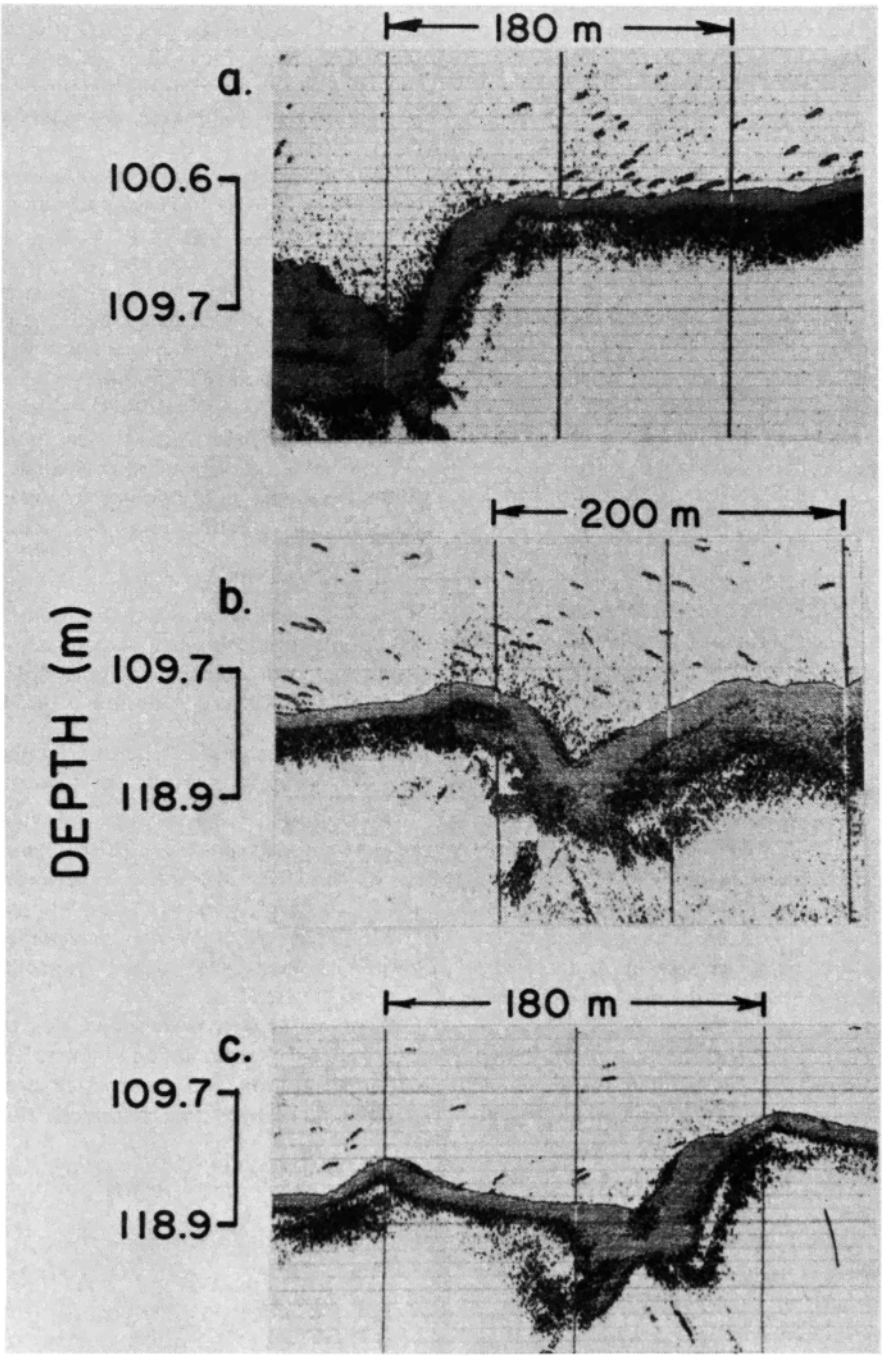

Fig. 5. The 200-kHz acoustic images of the discharge plume along (*a*) line 79, (*b*) line 80, and (*c*) line 67 (see Figure 1 for line locations). Note that the receiver gain was lower for the image shown in Figure 5*c*.

and the overlying fluid. We begin by deriving a set of governing equations which represent the approximate behavior of the mean flow and which is then further simplified by using the available data to show that certain terms are unimportant. It is then shown that at a fixed point a relation exists between volume transport and friction coefficient, and these quantities are estimated from the data. Finally, the downstream changes in continuous flow parameters are investigated.

5.1. *Governing Equations*

For simplicity, vertical and lateral uniformity in suspended sediment concentration and velocity are assumed. This approach assumes implicitly that the dynamics of the system are well represented by mean values and is examined in more detail in Appendix 1. The approach has the important advantage that the vertical dependence of the turbulent fluxes is removed, and experimental determinations of drag coefficients and entrainment rates for two-dimensional density currents can be introduced.

The slope of the interfacial region in the acoustic image in Figure 4 suggests a cross-stream momentum balance between the Coriolis and centrifugal accelerations and the cross-stream pressure gradient, as assumed by *Komar* [1969] and *Bowen et al.* [1984]. For leftward curving channels in the northern hemisphere in which the channel width W is much less than the radius of curvature r_0 this balance takes the form, after

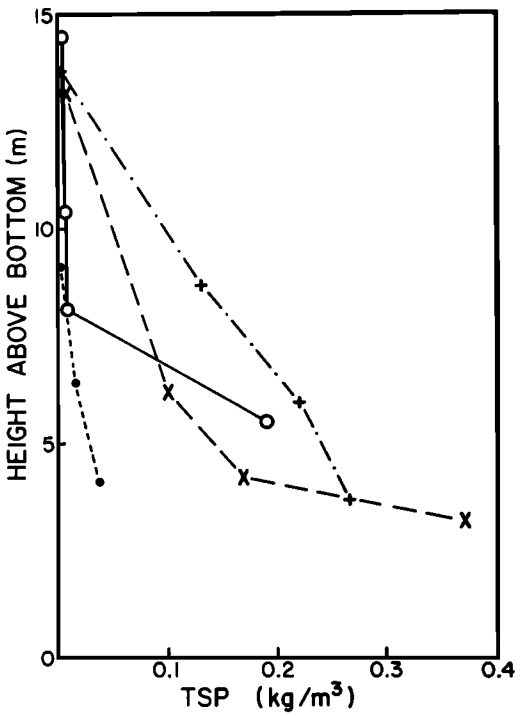

Fig. 6. Suspended sediment concentration profiles during the meandering channel phase in November 1976 at station D (Figure 1). The different symbols represent different profiles.

making the Boussinesq approximation,

$$fu + \frac{u^2}{r_0} = \xi g M \frac{\Delta h}{W} \tag{1}$$

where u is the speed in the streamwise direction, f the Coriolis parameter, $\Delta h/W$ the cross-stream interfacial slope, M the mass concentration of suspended sediment, and

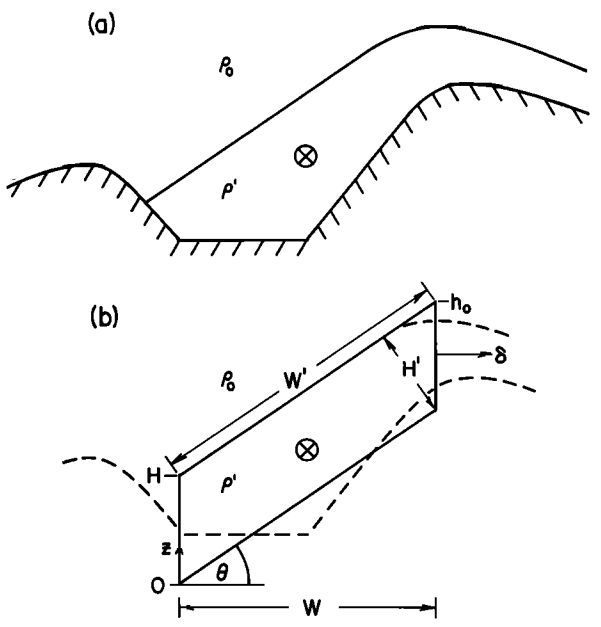

Fig. 7. (*a*) Schematic cross-channel profile and (*b*) definition sketch of the control volume for the cross-stream averaged model, shown superimposed on the cross-channel profile (dashed line) taken from Figure 7*a*. The encircled crosses in Figures 7*a* and 7*b* denote the direction of the mean flow u (into the plane of the drawing).

$$\xi = \frac{\rho_s - \rho_0}{\rho_s \rho_0} \tag{2}$$

The grain density of the suspended particles is ρ_s, and ρ_0 is the density of the ambient seawater. The excess density of the flow is given by

$$\frac{\Delta\rho}{\rho_0} = \xi M \tag{3}$$

Since the inertial acceleration terms in (1) do not depend explicitly on the radial coordinate r, it is clear that u should be independent of r for a constant cross-stream interfacial slope. The acoustic image in Figure 4 suggests that this should be a reasonable approximation, especially considering the degree of vertical exaggeration. The flow geometry is sketched in Figure 7*a* and has been simplified for the present analysis as shown in Figure 7*b*. The flow thickness H has been taken to be independent of r and may be thought of as the cross-stream-averaged flow thickness. Similarly, θ is the cross-stream-averaged bottom slope.

Consider conservation of downstream momentum in the control volume sketched in Figure 8. The downstream distance is $x = r_0\phi$, where ϕ is the azimuthal angle. Again invoking the Boussinesq approximation and referring to Figure 8, the downstream momentum balance is

$$(W'H'u)u_x + (W'H'u)_x u = \xi g M W' H' \sin\beta - \frac{(\tau_0 + \tau_i)}{\rho_0} W' - u\delta - \frac{MuWw_s}{\rho_0} \tag{4}$$

where τ_0 and τ_i are the bottom and interfacial shear stresses, respectively. The subscript x denotes partial differentiation

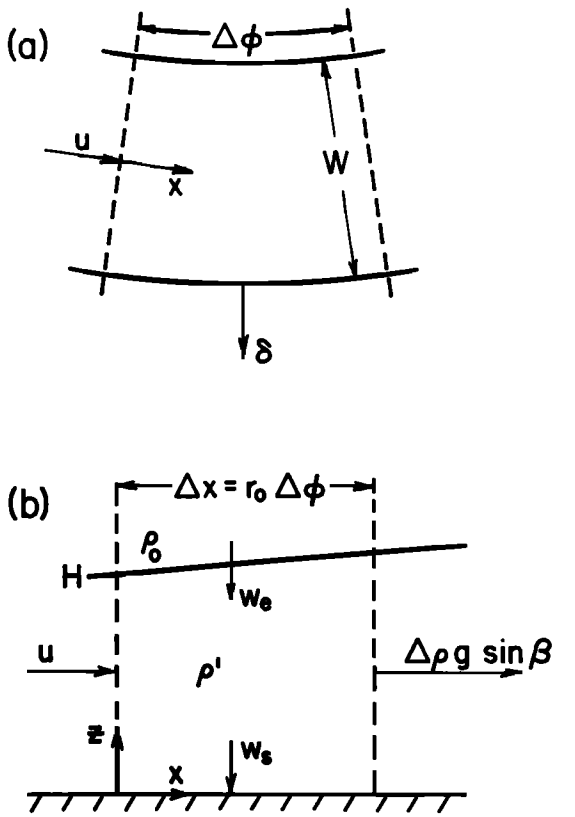

Fig. 8. Definition sketches of the control volume (*a*) in plan view and (*b*) in the along-channel direction.

with respect to x. The bottom slope in the along channel direction is tan β. The last two terms on the right-hand side in (4) represent the loss of downstream momentum due to channel overspill and deposition, respectively; δ is the volume rate of overspill per unit downstream distance, and w_s is the effective sedimentation velocity.

The equation for conservation of sediment is

$$(MW'H'u)_x = -WMw_s - M\delta \tag{5}$$

so that the divergence of downstream sediment transport is caused by sedimentation and channel overspill. Similarly, the equation for conservation of volume is

$$(W'H'u)_x = Ww_e - \delta - \frac{M}{\rho_s} Ww_s \tag{6}$$

where the last term is the volume loss due to sedimentation. The entrainment of fluid at the upper interface is parameterized in terms of an entrainment velocity w_e, taken to be positive downward. In this paper we use the formulation given by *Bo Pedersen* [1980*a*, *b*]

$$w_e = 0.072 \sin \beta\, u \tag{7}$$

the important features of which are the linear dependence on bottom slope and velocity. Equations (5) and (6) are similar to the continuity equations (3) and (4) given by *Komar* [1973], but differ in that sediment and volume, rather than sediment and water, are conserved separately, and in that overspill is included.

Equations (4)–(6) may be written in more convenient form by noting that $W'H' = WH$ and $W = W' \cos \theta$ (Figure 7*b*), and by using (6) to eliminate $(W'H'u)_x$ from (4). We therefore have the downstream momentum equation

$$\xi gMH \sin \beta = \frac{\tau_o + \tau_i}{\rho_o \cos \theta} + u(w_e + \xi Mw_s) - Huu_x \tag{8}$$

and the two scalar conservation equations

$$(MWHu)_x = -WMw_s - M\delta \tag{9}$$

$$(WHu)_x = Ww_e - \delta - \frac{M}{\rho_s} Ww_s \tag{10}$$

Note that overspill does not enter the downstream momentum balance (8). Moving fluid is extracted from the turbidity current, reducing the volume transport. No exchange of fluid occurs, however, so there is no associated drag.

Consider the sedimentation term in (8). Let w_* be the terminal settling velocity of individual grains, assumed to be given by the Stokes settling velocity for a sphere [e.g., *Batchelor*, 1967 p. 234]. A typical mean diameter for the suspended tailing is 14 μm [*Hay*, 1983], giving $w_* \approx 1.8 \times 10^{-2}$ cm s^{-1}. Because of turbulent diffusion away from the high concentration region next to the bed it is to be expected that

$$w_s \leq w_* \cos \beta \tag{11}$$

where the cos β term arises because the direction normal to the bed is not vertical. The ratio of the sedimentation and entrainment terms in (8) is therefore less than or nearly equal to

$$\frac{\xi Mw_*}{0.072 \tan \beta u} \approx 3.5 \times 10^{-5}$$

where values of $\beta = 2.2°$, $\rho_s = 2.7 \times 10^3$ kg m^{-3}, and $M = 0.25$ kg m^{-3} (Figure 6) have been used. In addition, a velocity scale $u = 30$ cm s^{-1} was chosen, since this will be shown to be typical of the expected speeds. The loss of momentum due to deposition is therefore small in comparison with that due to entrainment, and the w_s term in (8) may be dropped.

Similarly, sedimentation has a negligible effect on volume conservation. From (7), $w_e \approx 8.2 \times 10^{-2}$ cm s^{-1} for a 30 cm s^{-1} flow speed, which is comparable to w_* (1.8×10^{-2} cm s^{-1}). Since $M \ll \rho_s$, it is clear comparing the w_s and w_e terms in (10) that volume change due to deposition is much less than that due to entrainment, and the w_s term will therefore be neglected.

Finally, the nonlinear term Huu_x in (8) is ignored. This assumption has been made in previous models of continuous turbidity current flow in curved channels [*Komar*, 1969, 1973; *Bowen et al.*, 1984]. Its validity in the present context will be judged by comparing the linear theory to observation. The governing equations (1), (8), (9), and (10) therefore become

$$fu + \frac{u^2}{r_0} = \xi gM\left(\frac{h_0 - H}{W}\right) \tag{12a}$$

$$u^2 = \left(\frac{2\xi g \sin \beta}{f''}\right)(MH) \tag{12b}$$

and

$$HuM_x = -M(w_s + u_e) \tag{13a}$$

$$(WHu)_x = Ww_e - \delta \tag{13b}$$

Equation (13*a*) was obtained by substituting (13*b*) in (9). Equation (8) has been rewritten in the Chezy-type form (12*b*) by assuming the usual quadratic speed dependence in the stress terms

$$\frac{\tau_0 + \tau_i}{\rho_0} = \frac{f_*}{2} u^2 \tag{14}$$

f_* being a composite drag coefficient (including both interfacial and bottom friction), and by using (7) to eliminate the entrainment velocity. The effective drag coefficient f'' is given by

$$f'' = \frac{f_*}{\cos \theta} + 0.144 \sin \beta \tag{15}$$

Overspill appears explicitly only in the volume conservation equation, deposition only in the sediment conservation equation.

It is convenient to define the volume transport

$$Q = WHu \tag{16}$$

and to solve (12) for u and M in terms of Q and H. Using (12*b*) to eliminate u from (12*a*), we find that

$$M^{1/2} = \left(\frac{f''}{2\xi gH \sin \beta}\right)^{1/2} r_0 f\left[\frac{r_0 f''(h_0 - H)}{2WH \sin \beta} - 1\right]^{-1} \tag{17}$$

By using (16) to eliminate WH from (17) and substituting the result in (12*b*), a quadratic equation in u is found for which the solution is

$$u = \frac{\sin \beta}{r_0 f''} \frac{Q}{(h_0 - H)} \left\{1 + \left[1 + \omega\left(\frac{h_0 - H}{Q}\right)\right]^{1/2}\right\} \tag{18}$$

where the positive root has been taken in order that u remain

positive for $H < h_0$ and where

$$\omega = \frac{2r_0{}^2 ff''}{\sin \beta} \tag{19}$$

Equation (17) becomes

$$M^{1/2} = \left(\frac{f''}{2\xi g \sin \beta}\right)^{1/2} 2r_0 f \left\{H^{1/2}\left[\left(1+\omega\left(\frac{h_0-H}{Q}\right)\right)^{1/2}-1\right]\right\}^{-1} \tag{20}$$

5.2. *Estimating f″ From Conditions at x = 0*

The origin ($x = 0$) in this analysis is taken to be the location of the cross-channel profile shown in Figure 4, which is about two thirds of the way along the constant slope section of the upper reach (see Figures 1 and 2). At $x = 0$, $u = u_0$, $H = H_0$ and $Q = Q_0$, where

$$Q_0 = W_0 H_0 u_0 \tag{21}$$

By using (18) to substitute for u_0 in (21), the following relation is obtained:

$$Q_0 = r_0 f W_0 H_0 \left[\frac{r_0 f''}{2 \sin \beta}\left(\frac{h_0 - H_0}{W_0 H_0}\right) - 1\right]^{-1} \tag{22}$$

Equation (22) is a key result in the present development, since it relates the only two quantities for which no observations exist: Q_0 and f''. It is shown below that quite narrow bounds can be placed on the possible values of Q_0 and f''.

From Figure 4 it is estimated that $h_0 - H_0 = 3.5$ m, $H_0 = 8.8$ m, and $W_0 = 62$ m. Using $f = 10^{-4}$ s^{-1}, $r_0 = 1300$ m and $\beta = 2.2°$ (see section 3); values of Q_0 were calculated using (22) for various values of f'' and are listed in Table 2. Also shown in Table 2 are the values of u_0 and M_0 determined from (18) and (20), respectively, and the values of suspended sediment transport $M_0 Q_0$, the square of the densimetric Froude number ($F_r{}^2 = u_0{}^2/g'H_0$), and the friction coefficient f_*.

Since the sediment mass transport in a depositional system cannot exceed the rate of discharge (380 kg s^{-1}), and since the total transport must include both bed load and surge transport in addition to the suspended load transport estimates in Table 2, small values of f'' (<0.011) may be eliminated. This conclusion is consistent with the fact that the calculated values of M_0 for values of f'' below 0.011 are much greater than those observed (Figure 6). Furthermore, large values of f'' (>0.016) yield estimates of M_0 much smaller than those observed.

The values of the friction coefficient in Table 2 are to be compared with those reported for density currents. *Bo Pedersen* [1980*a*, p. 95, 1980*b*, Figure 1] has plotted the bulk Richardson number $Ri = 1/F_r{}^2$ against sin β for the available experimental data. From (12*b*),

$$Ri = \frac{f''}{2 \sin \beta} \tag{23}$$

which represents the usual dependence of Ri on bottom slope and friction, except that here f'' is a modified friction coefficient. If it is assumed that (12*b*) implies that f'' will have roughly the same dependence on axial bottom slope and Richardson number as do the friction coefficients for density currents, then Bo Pedersen's compilation suggests that $10^{-2} < f'' < 10^{-1}$. The values of f'' in Table 2 fall in this range but are closer to 10^{-2}.

5.3. *Entrainment-Driven Overspill*

Having arrived at a set of governing equations and a best estimate for the range of values of f'', we are now in a position to investigate changes with distance downstream and, in particular, the effects of overspill and sedimentation. One candidate overspill mechanism is the increased volume transport caused by entrainment. Assuming that overspill is driven solely by entrainment, then

$$\delta = W w_e \tag{24}$$

so that (13*b*) becomes

$$WHu = Q_0 \tag{25}$$

where the volume transport Q_0 is constant. It can be seen immediately from (25) that entrainment-driven overspill can produce the downstream reduction in channel cross section (WH) only if there is a corresponding downstream acceleration of the mean flow, which is unreasonable.

5.4. *Sedimentation*

Sedimentation effects are not easily incorporated into turbidity current models explicitly, since the dependence of the effective sedimentation velocity on flow parameters is not well understood. In the present instance, however, it is possible to show that to a first approximation, sediment deposition can be ignored. A length scale L_M for the downstream change in concentration can be defined from (13*a*) such that

$$L_M \approx \frac{Hu}{w_s + w_e} \tag{26}$$

where H and u are typical thickness and velocity scales. Equation (26) holds provided H and u vary slowly with distance downstream. It can be shown, although it requires some effort, that this is to be expected in a channel with constant relief (e.g., $h_0 = \text{const}$) and constant slope when (24) holds. Furthermore, u and H are found to vary slowly for the other overspill mechanism considered here as well. Returning to (26), we find that for $H \sim 10$ m, $u \sim 30$ cm s^{-1}, and $w_s + w_e \sim 10^{-1}$ cm s^{-1}, $L_M \sim 3$ km. This is much longer than the few hundred meters of the upper reach that are of interest here, suggesting that the changes in M are unlikely to be very large. Finally, since $w_s \sim w_e/4$, sedimentation will make a small contribution to an already small change and will be ignored. Equation (13*a*) is accordingly rewritten in the form

$$HM_x = -0.072 \sin \beta \, M \tag{27}$$

5.5. *Inertial Overspill*

The question remains as to how to deal with the overspill term δ in the volume transport equation (13*b*). The previous

TABLE 2. Calculated Flow Parameters at $x = 0$ as a Function of f''

f''	Q_0, m^3 s^{-1}	u_0, m s^{-1}	M_0, kg m^{-3}	M_0Q_0, kg s^{-1}	f_*, $\times 10^{-3}$	$F_r{}^2$
0.010	731	1.34	4.35	3180	4.1	7.6
0.011	343	0.629	1.05	361	5.0	6.9
0.012	224	0.411	0.491	110	5.9	6.3
0.013	166	0.305	0.293	48.7	6.8	5.8
0.014	132	0.243	0.200	26.4	7.3	5.4
0.015	110	0.201	0.147	16.2	8.6	5.1
0.016	93.9	0.172	0.115	10.8	9.5	4.7
0.017	82.0	0.150	0.093	7.6	10.5	4.5

discussion indicates that the downstream decrease in channel cross section is not a morphology compatible with the continuous flow alone. It is therefore useful to consider whether this morphology might result from levee slumping and surge-type flow. In this view the leftward curvature and narrowing cross section of the channel are prescribed as far as the continuous flow is concerned. A tendency for the fluid columns to climb the outer bank could then arise if the radius of curvature of the outer levee crest were smaller than that of the channel axis, r_0 (as suggested by Figure 1). In other words, the balance between the inertial terms and the pressure gradient in (1) would be satisfied only if the fluid columns followed paths with radii of curvature equal to r_0, which requires that columns over the outer bank, where the radius of curvature of the channel bottom is less than r_0, gradually climb toward and spill over the levee crest as they move along channel. The term "inertial overspill" is therefore suggested for this process, which is sketched in Figure 9. It can be seen that the volume rate of overspill per unit length of channel will be given approximately by

$$\delta \approx -H \frac{dW}{dx} u \tag{28}$$

where the negative sign is required because δ is positive for $dW/dx < 0$. Equation (13*b*) becomes

$$(WHu)_x = u\left(0.072 \sin \beta\, W + H \frac{dW}{dx}\right) \tag{29}$$

The ratio of the overspill and entrainment terms in (29), for $dW/dx = -0.2$ (Figure 2*c*), $W = 62$ m, $H = 8.8$ m, and $\beta = 2.2°$, is about 10. This is large enough that the entrainment term can be ignored, and (29) reduces to the simple form $(Hu)_x = 0$, or

$$Hu = H_0 u_0 \tag{30}$$

It is important to note that this result implies that the inertial overspill rate is constant along the length of the channel. Combining (30) with (12*b*) gives

$$M = M_0 \frac{H_0^3}{H^3} \tag{31}$$

which, when substituted in (30), gives $H_x = 0.024 \sin \beta$ or,

$$H = H_0 + 0.024 \sin \beta\, x \tag{32}$$

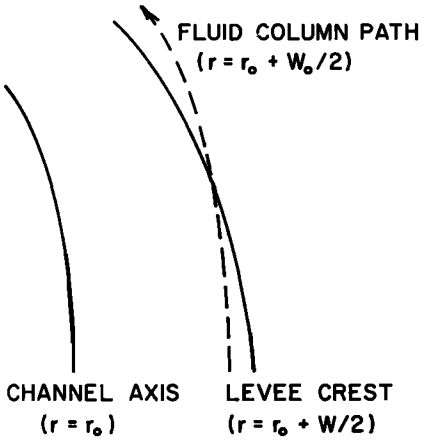

Fig. 9. Sketch showing the path of a fluid column in plan view undergoing inertial overspill.

TABLE 3. Inertial Overspill: Bulk Flow Parameters at $x = 150$ m Near the End of the Upper Reach

f''	u, m s^{-1}	Q, m^3 s^{-1}	M, kg m^{-3}	MQ, kg s^{-1}
0.011	0.619	177	1.00	178
0.012	0.405	116	0.469	54.2
0.013	0.300	85.9	0.280	24.0
0.014	0.239	68.4	0.191	13.1
0.015	0.198	56.6	0.140	7.9

H increases linearly with distance downstream. From (30) and (31), both u and M decrease with x. W, of course, is prescribed.

The predicted flow parameters for $x = 150$ m at the bottom of the linearly narrowing section of the upper reach are presented in Table 3. Comparing these values to the $x = 0$ estimates in Table 2, it is seen that M and u exhibit small decreases, about 5 and 2%, respectively. From (32) the increase in H is 0.14 m. As before, therefore, the errors introduced by ignoring sedimentation are not expected to be important. In order to test the inertial overspill model the flow parameters were calculated for $x = -350$ m at the entrance to the linearly narrowing section and are given in Table 4. One of the features of the inertial overspill model is that it is consistent with the narrow range of friction coefficients chosen in section 5.2. For example, the mass transport MQ at $x = -350$ m exceeds the discharge rate at the outfall for $f'' \leq 0.011$. Similarly, for values of $f'' \geq 0.015$ the vertically averaged concentrations M are much lower than indicated by the measurements near $x = -350$ m (Figure 6; see also Figure 1). This suggests that the probable range of values of f'' is 0.012–0.014, which is within and somewhat narrower than the range determined previously.

The predicted overspill rates can be compared with the observed sediment accumulation rate in the vicinity of the right (west) levee. We assume that all of the overspilled tailing is deposited in the area immediately to the west of the linearly narrowing section of the upper reach, and north of the meander reach. The east-west dimension of this area is to be selected and is designated by l_0. The north-south dimension l_1 is set equal to 500 m, the length of the linearly narrowing section of the upper reach. Taking l_0 to be 300 m (see Figure 3*c*), the mean accumulation in this area was about 12 m during the period from the beginning of discharge in October 1971 until the survey in January 1977, or about 2.3 m yr^{-1}. The sediment accumulation rate calculated from the rate of overspill is

$$S = \frac{\Delta MQ}{\rho_B l_0 l_1} \tag{33}$$

where $\rho_B = 1.3 \times 10^3$ kg m^{-3} is the dry bulk density of the

TABLE 4. Inertial Overspill: Calculated Flow Parameters at $x = -350$ m at the Top of the Linearly Narrowing Section of the Upper Reach

f''	u, m s^{-1}	Q, m^3 s^{-1}	M, kg m^{-3}	MQ, kg s^{-1}	ΔMQ, kg s^{-1}	S, m yr^{-1}	R, kg s^{-1}
0.011	0.653	731	1.17	858	...	...	...
0.012	0.427	477	0.549	262	208	33.6	193
0.013	0.317	354	0.328	116	92.1	14.9	76
0.014	0.252	282	0.224	63.1	50.0	8.1	35
0.015	0.209	233	0.164	38.4	...	...	...

deposited tailing as before. ΔMQ is the inertial overspill loss in the linearly narrowing section of the upper reach, which is equal to the difference between the values of MQ at $x = -350$ m and $x = 150$ m in Tables 4 and 3, respectively. The values of ΔMQ and estimates of S from (33) are also listed in Table 4. The estimated accumulation rates are much too large, indicating that a large fraction of the overspilled material must be transported out of this area if the inertial overspill model is to be retained. This amount is designated by R and is listed in Table 4 for the selected probable range of friction coefficients. It is seen that roughly 70–90% of the overspilled material must be transported elsewhere if the observed accumulation rates are to be accounted for. Two mechanisms are likely to be important. One is the removal of deposited material by surge type flows, about which more will be said in section 6. In addition, the overspilled tailing must itself flow away from the levee crest as a broad unconfined turbidity current.

The second mechanism cannot by itself account for the difference. This can be seen from Figure 3*c*. The area of deposition can be extended westward on the north side of the meander reach for at most 1500 m, reducing the estimated accumulation rates in Table 4 by only a factor of 5. Yet from Figure 3*c* the observed average accumulation rate in this extended depositional area is about 6 m during the 5.25-year period of operation prior to the survey, or about 1.1 m yr^{-1}. The only overspill rate which approaches this value when corrected by the factor of 1/5 is that for $f'' = 0.014$. Furthermore, this neglects the contributions to deposition in the area from continuous and surge-type flows in the meander reach, and from the overspill from the steep section of the upper reach near the outfall.

6. Discussion

6.1. *Surge Recurrence Frequency*

In the discussion of the sediment accumulation budget in section 3 it was found that 240 kg s^{-1} of tailing had to be transported out of the proximal zone. The results of section 5 can be used to show that continuous turbidity current flow can contribute little to this transport.

Consider continuous flow in the lower reach at the position of the line YY' in Figure 3*c*. The channel is essentially straight, the axial slope angle $\beta = 0.47°$, and the relief and width of the channel are typically 5 m and 80 m, respectively, in this vicinity (Figure 2). Because the channel is not curved, the discussion of mean flow dynamics in section 5 suggests that $f_* + 0.144 \sin \beta$, not f'', should be used in (12*b*). Taking $f'' \approx 0.013$, f_* is about 7×10^{-3} (Table 2). Finally, since it has been shown that suspended sediment concentrations change slowly with distance downstream, we assume that the concentration in the lower reach is comparable to, or smaller than, that in the upper reach, that is, $M \leq 0.25$ kg m^{-3}. Then, from (12*b*), with $H = 5$ m (the channel relief),

$$u \approx 0.11(MH)^{1/2} \tag{34}$$

from which $u \approx 0.13$ m s^{-1} and

$$MQ \approx 13 \text{ kg s}^{-1}$$

One could justifiably double this value to account for the bedload transport in the channel and the additional suspended load transport above and outside the channel, but this still leaves some 210 kg s^{-1} to be transported out of the proximal zone. We note that this value is of the same order of magnitude as the fraction R of the inertial overspill which would have to be removed from the upper reach to reconcile the observed and predicted accumulation rates (Table 4).

The suggestion is therefore made that surge-type turbidity currents resulting from levee failure in the upper reach are responsible for the missing transport. An estimate of the transport by surge-type flows can be made. The speed of a surge is given by [*Hay*, this issue]

$$U_* = 0.75[g'H_*]^{1/2} \tag{35}$$

where H_* is the head thickness and $g' = (\Delta\rho/\rho_0)g$ is the reduced gravity. For a surge which lasts a time T the excess mass transported is given approximately by MWH_*U_*T. An appropriate scale for the excess density was shown by *Hay* [this issue] to be 100 kg m^{-3}, giving $M \sim 160$ kg m^{-3} (equation (3)). The head thickness is set equal to the depth of the channel in the lower reach (5 m). This assumption is consistent with the acoustic images of the 1976 Rupert Inlet surge reported by *Hay et al.* [1982]. Equations (3) and (35) therefore give $U_* \approx 1.3$ m s^{-1}. With $W = 80$ m, the mass of tailing transported within the channel per surge becomes

$$8.4 \times 10^4 T \text{ kg}$$

where T is the duration (in seconds) of the surge at a fixed point. The duration of the high concentration head and shrinking body region is about 5 min. The mass of material transported per event is therefore about 2.5×10^7 kg.

In order that such events remove 210 kg s^{-1} from the proximal zone they must recur on average at intervals of about 1.4 days. Considering the uncertainties involved, this is in very good agreement with the recurrence interval of 2–5 days determined from turbidites found in cores from the levees [*Hay et al.*, 1983*b*]. Three factors could contribute to the difference. The calculated recurrence interval is based on surge observations made during the apron phase. These surges might be smaller than those produced by slumping of the steeply inclined levees in the upper reach during the meandering channel phase when the cores were taken. The second factor is that the recurrence interval observed in the cores is based upon the thicker, more readily identifiable turbidite layers and is therefore biased toward larger values. Finally, the contribution of the inlet circulation to the transport has not been considered. This quantity is estimated in Appendix 2 to be between 30 and 60 kg s^{-1}. This gives a revised surge transport rate of 150–180 kg s^{-1} and a recurrence interval in the range 1.6–1.9 days.

6.2. *Levee Failure, Left Hooking in the Upper Reach, and the System Overall*

The most likely source region for the surges is the upper reach. The levees in the upper reach consisted primarily of sand and silt similar in size and metal content to that found in the coarse-grained turbidites farther downchannel [*Hay et al.*, 1983*b*]. Furthermore, the channel banks are steep and the deposition rates are high in this area, and the axial slope of the channel itself is steeper than elsewhere.

The amounts of overspilled material (R in Table 4) which must be removed from the levee area to obtain reasonable predicted accumulation rates are of the same order of magnitude as the surge transport rate estimated above. Closer correspondence would probably be obtained if a rate of removal by surges generated in the steep section of the upper reach near the outfall were estimated and added to R. Exact

agreement would not be expected in any case; however, the net transport by surge-type flow from the generation region in the upper reach is unlikely to equal that from the proximal zone at the end of the meander reach. Erosion and deposition along the intervening length of channel are bound to cause differences. The degree of similarity which does exist between the values of R and the 150–180 kg s^{-1} transported by surges from the proximal zone therefore provides additional support for the inertial overspill model.

On balance, therefore, the morphology of the upper reach cannot represent a state in slowly changing equilibrium with the continuous flow alone. Instead, it appears that the channel in this reach is shaped by levee failure and subsequent surge flow, and this shape guides but does not fully contain the continuous flow. Once formed, the persistence of a left hook would be assured in the inertial overspill model because the deposition rate would necessarily be larger on the right and therefore so would the rate of levee failure. It is suggested that the surges would carry material away from the right levee at more or less the rate at which it was deposited and at the same time would no doubt erode material from the left bank at the base of the upper reach due to the rightward curvature of the channel there. (Note that rightward curvature at the base of the upper reach is a necessary outcome of the inlet bathymetry.) If this interpretation is correct, then the origin of the left hook in the Rupert Inlet channel is unlike that proposed by *Menard* [1955] for submarine channels in the deep ocean, in which levee failure along the length of the channel played no role.

We are left therefore with a description of the system which is appealing both because it is self-consistent and physically reasonable. For example, we expect that surge-type flows should carry material farther than continuous flow. Consistent with our expectations, we find that turbidites form an increasingly important fraction of the sediment column with distance downchannel [*Hay et al.*, 1983*a*]. Furthermore, we find that nearly half of the material discharged must be transported out of the proximal zone but predict that the continuous flow and the inlet circulation can account for only a part of this. The remainder must be transported by surge-type flow, and we find that the surge recurrence frequency based on this residual and the estimated excess mass per surge is consistent with the recurrence frequency determined from turbidites in cores. We expect that levee failure resulting in channelized surges should occur predominantly in the upper reach. We find that the predicted rates of overspill from the continuous flow in the upper reach are such that the observed accumulation rates can be accounted for only if levee slumping and surge-type flow remove a large fraction of the overspilled material. Furthermore, the amounts which are overspilled and which must be removed are of the same order as the surge transport rate into the distal zone. Finally, the predictions of the continuous flow model are consistent with the constraints imposed by the known rate of discharge and the observed suspended tailing concentrations.

Now consider the meanders. The probable sediment and volume transports by continuous and surge-type flows through this reach will be taken as measures of the relative importance of each to meander development. Consider the sediment transports first. The surge output rate is 150–180 kg s^{-1}. Examining Table 4, we see that the only compatible value of R is 193 kg s^{-1}, for which $f'' = 0.012$. R is equivalent to the surge input rate. From Table 3 the predicted input from continuous flow is 54 kg s^{-1}. Using the same assumptions as before, the continuous transport corresponding to channel full flow in the lower reach for this value of f'' and $M = 0.5$ kg m^{-3} would be 40 kg s^{-1}. The surge flow transport through the meander reach is therefore 3–4 times that due to continuous flow. One might conclude that this implies that the surges must be primarily responsible for meander development, but this may not be so. The reason is that the volume transport into the meander reach by the continuous flow is much greater than that by the surges. From Table 3, Q is 116 m^3 s^{-1} for $f'' = 0.012$. This is the volume transport by continuous flow into the meander reach. That by surge-type flow, from $R = 193$ kg s^{-1} and $M = 160$ kg m^{-3}, is only about 1 m^3 s^{-1}. This should certainly be increased by the volume transport in the low concentration wake, but this too cannot be large. For example, if we take $M = 0.5$ kg m^{-3}, which is consistent with *Hay* [this issue], and assume that the same overspill dynamics apply to the wake as to the continuous flow, then the wake transport into the meander reach would be 116 m^3 s^{-1}. This transport only lasts for about an hour every second day, however, so it is small.

The meander formation problem is beyond the scope of this paper. The relative importance of the frequent high-speed, sediment-laden surges compared to the slow but steady continuous flow is left as an open question. Some resolution of the question might be sought in the behavior of subaerial river channels, but there are difficulties with applying this analogy directly. Unlike rivers, the continuous flow overspills the channel levees continuously. Furthermore, the surges are not analogous to flood stages in rivers: They are bores, not waves. One thing is clear. The downstream increase in the importance of turbidites in the sediment column on the levees indicates that the continuous flow contributes less and less to the channel building process. Much of this downstream waning can be attributed to overspill in the meander reach, where mud layers are much thicker than the intervening coarse-grained turbidites.

6.3. *Inertial Overspill and Flow Stripping*

A distinction is drawn between the flow-stripping mechanism proposed by *Piper and Normark* [1983] and discussed by *Bowen et al.* [1984] and the inertial overspill mechanism discussed here. Flow stripping occurs when a turbidity current which is thicker than the channel is deep encounters a sharp bend. That portion of the current higher than the levees is unimpeded by the bend and is "stripped off," while the lower and now less thick portion continues along the channel. The current splits into two parts, one following the channel and the other flowing outside the channel in the same direction as the current upstream. This process is readily imagined for surge-type flows, particularly where the head encounters a sharp bend and sheds an overspill surge over the levee crest. Such an overspill event was described by *Hay et al.* [1982].

Inertial overspill, on the other hand, occurs whenever the curvature in plan view of the outer bank in a channel bend is greater than that of the channel axis. The fluid columns in the current are carried up the bank and over the levee by their forward momentum. It is not required that the bend be sharp. Separation of that part of the current which overflows the levee and that part which remains in the channel does not necessarily occur. Neither is there an abrupt reduction in the thickness of the channelized part of the flow. So, while it is

clear that flow stripping is also an inertial effect, the two processes are quite different.

6.4. *Sediment Deposition Revisited*

In section 5 it was shown that sedimentation within the channel does not contribute to the mass balance in the upper reach. This conclusion was based on a mean particle diameter of 14 μm, however, which leads to two problems. The first is that the distribution of particle sizes was not considered, which is potentially dangerous because the Stokes settling velocity depends on the square of the particle size. The second is that this mean size was based on samples taken from the discharge plume at a distance of 400 m from the outfall [*Hay*, 1983] and is half the median size of the tailing discharged (30 μm). The implication is that the larger particles settled out before reaching the sampling site.

The size distribution of discharged tailing is reasonably broad: 50% of the particles are coarser than 30-μm diameter, and 25% are coarser than 100-μm diameter. The settling velocity for a 100-μm particle is about 0.9 cm s^{-1}. This means, for example, that such a particle would settle through the 8-m-thick, 30 cm s^{-1} mean flow after an axial displacement of only 260 m. Even if the turbulent flux of sediment away from the bed were known and could be included, one suspects that settling of the coarser-grained particles must be important. This suspicion is confirmed by the downstream fining of the sediments in suspension implied by the 14-μm mean size determination and by the downstream fining of the sediments deposited on the levees [*Hay et al.*, 1983*b*].

The probable importance of sedimentation of the coarser fraction has desirable consequences.

1. The coarsest material will settle out high in the upper reach, providing the required source of coarse-grained material for the turbidites found in the distal zone.
2. The tailing mass transport MQ required of the continuous flow in the upper reach is reduced by the amount of sedimentation which occurs. Examining Table 2, for example, one sees that a 25% loss through deposition excludes all values of $f'' < 0.012$, reinforcing previous conclusions.
3. Further reductions in mass transport by continuous flow in the upper reach provide additional support for the argument that surge-type flows are the primary sediment transport mechanism farther downstream.
4. Settling of the coarser fraction both onto the right bank from the continuous flow and onto the right levee from the overspill will produce the high local deposition rates required to have a mass balance between accumulation from the continuous flow and relatively localized removal by slump-generated surges.

The arguments with respect to sedimentation in section 5.1 must be reexamined, however. It is clear that even if w_* is increased by 2 orders of magnitude (corresponding to $D = 140$ μm), the sedimentation term in (8) remains small and the same is true of (10). The governing equations (12) and (13) are therefore unaffected, and the effects of sedimentation loss still depend on the relative size of w_s and w_e. In section 5 it was effectively assumed that the coarsest particles settle out high in the upper reach and that the effective sedimentation rate w_s for the remaining fine-grained material is small. This approach is supported by the fact that the turbulent flux of sediment away from the bed produces a reduction in w_s and may in some cases achieve a state of autosuspension as proposed by *Bagnold* [1962]. Rather than rely on the existence of such a state I have assumed that the effective sedimentation velocity w_s remains small for a substantial fraction of the tailing or, more precisely, that it remains smaller than the entrainment velocity w_e.

7. SUMMARY AND CONCLUSIONS

Acoustic images of the continuous turbidity current flow associated with the discharge show it to be detectable to distances at least as great as 2 km from the outfall, that is, nearly to the end of the meander reach. Where the channel is curved, the continuous flow is seen to be concentrated against the outer bank and to spill over the crest of the outer levee. Flow thickness and the cross-channel interfacial slope are obtained directly from the images.

A model for continuous turbidity flow in a narrow, left-hooking channel with constant axial slope is presented. The model includes entrainment, sediment deposition, and the effects of mass loss through channel overspill. The known rate of tailing discharge and the observed suspended particulate concentrations within the channel are used together with observed accumulation rates as constraints to estimate the probable range of friction coefficients. This range turns out to be quite narrow.

The channel cross section throughout most of the upper reach decreases with increasing distance from the outfall. By assuming that the decreasing cross section is the result of levee slumping and surge-type flow and that the continuous flow must therefore attempt to negotiate a prescribed channel shape, a simple inertial overspill model is derived. This model provides reasonable estimates of suspended tailing concentration and transport but predicts a rate of overspill which would result in accumulation rates greater than those observed. The model results can be reconciled with observation, however, if the excess accumulation is assumed to be removed from the upper reach by slump-generated surge-type flows.

The surge transport rate is estimated independently from a sediment accumulation budget derived from seismic profiling surveys. By dividing the tailing deposit into proximal and distal zones it is determined that 240 kg s^{-1} must be transported from the proximal into the distal zone. The continuous flow and the inlet circulation can account for at most 60–90 kg s^{-1}, leaving the remaining 150–180 kg s^{-1} to be transported by surges. This transport rate is verified independently by estimating the mean surge recurrence interval from the transport rate itself and the mass excess per surge obtained from *Hay* [this issue]. The recurrence interval determined in this way is about 2 days, which is remarkably consistent with the range of 2–5 days estimated from the number of coarse-grained turbidites in cores from the levees. Finally, this surge transport rate is the same order as the rate of removal from the upper reach required to reconcile the inertial overspill model with the observed accumulation rates.

A principal conclusion of the paper therefore is that except high in the upper reach, surge-type flow is responsible for most of the sediment transport. The left-hooking upper reach is the probable source region for the surges, the frequency of levee failure presumably being governed by the high rate of deposition and the steepness of the channel banks. The morphology in this reach apparently represents slowly changing equilibrium between deposition, resulting primarily from overspill, and levee failure.

The relative importance of continuous and surge-type flows in the formation of the meanders is not clear. Although sedi-

ment transport is dominated by surges, the continuous flow dominates volume transport. More work on the problem of meander formation by turbidity currents is needed, especially since this process is likely to differ in important ways from that in subaerial rivers. Differences are to be expected because turbidity currents are not confined by the channel banks and the dynamic equivalent of surge-type flow does not occur in rivers. It is clear, however, both from the calculations and the increasing importance of turbidites in the levee sediments with distance downstream that the continuous flow probably contributes little to channel building below the meander reach.

Tailing discharge systems like that in Rupert Inlet provide useful laboratories in which turbidity currents and the formation of submarine channels can be studied at scales which at least approach those of their deep-sea counterparts. The known rate of sediment input and ability to monitor the development of the deposit through time have been shown to provide overall constraints which are useful when investigating the dynamics of the system. Finally, it has been demonstrated that acoustic remote sensing techniques provide essential information about turbidity currents which would be virtually impossible to obtain in any other way.

APPENDIX 1: GOVERNING EQUATIONS

In section 5 the governing equations were derived by assuming that excess density and flow speed were uniform in the vertical and cross-stream directions. This assumption is now relaxed, and the governing equations are rederived from first principles.

Consider flow in a channel with radius of curvature r_0 at the channel axis. As before, the along- and cross-channel coordinates are $x = r\phi$ ($dx = rd\phi$) and r, respectively, and u is the along-channel velocity. We introduce the transverse (radial) velocity component v and the vertical velocity w. The continuity equation is [cf. *Batchelor*, 1967, p. 602]

$$u_x + \frac{v}{r} + v_r + w_z = 0 \tag{A1}$$

Let $z = -b(x, r)$ represent the bottom and $z = -b(x, r) + H(x, r)$ represent the interface between the turbidity (density) current and the ambient fluid. Note that the bottom b and the flow thickness H are allowed to vary with position arbitrarily, so that this approach is far more general than that used earlier. Integrating (A1) in the vertical and requiring that there be no flow through the bottom ($\mathbf{u} \cdot \nabla(z + b) = 0$ at $z = -b$) and that the flow through the interface equal the entrainment velocity w_e ($\mathbf{u} \cdot \nabla(z + b - H) = -w_e$ at $z = -b + H$) yields

$$(H\bar{u})_x + \frac{H\bar{v}}{r} + (H\bar{v})_r = w_e \tag{A2}$$

where the overbars denote vertical averages. Except for the entrainment term this is the same as the vertically integrated form of the continuity equation for river flow [cf. *Smith and McLean*, 1984, equation (5)].

We are interested in the laterally integrated form of (A2). Let the curve $r = r_0 + W_+(x)/2$ represent the outer bank and $r = r_0 - W_-(x)/2$ represent the inner bank. It is convenient to use positive and negative subscripts to denote the outer and inner banks. With the boundary conditions that there be no transport through the inner bank ($H_-\bar{v}_- = 0$) and a radial transport $H_+\bar{v}_+ = \delta$ at the outer bank due to overspill, (A2) when integrated across the width of the channel becomes

$$(W\langle H\bar{u}\rangle)_x = W\langle w_e\rangle - \delta - \int_{r_0 - W/2}^{r_0 + W/2} \frac{H\bar{v}}{r}\, dr \tag{A3}$$

where the angle brackets denote the cross-channel average. For narrow channels, $W \ll r_0$, and since $0 \le H\bar{v} \le \delta$, the integral is of order $\delta W/r_0$. This is much less than δ, and (A3) therefore becomes

$$(W\langle H\bar{u}\rangle)_x = W\langle w_e\rangle - \delta \tag{A4}$$

This is of the same form as (10), except for the sedimentation term which has not been included here.

Similarly, the equation for conservation of suspended sediment in cylindrical coordinates is

$$(Mu)_x + (Mv)_r + \frac{Mv}{r} + (Mw)_z = (Mw_s)_z \tag{A5}$$

where the Stokes settling velocity w_s is again positive downward. Integrating in the vertical from $z = -b$ to $z = -b + H$ as before but with $M = 0$ at the interface, this becomes

$$(H\overline{Mu})_x + (H\overline{Mv})_r + \frac{H\overline{Mv}}{r} = -M(-b)w_s(-b) \tag{A6}$$

Integrating in the horizontal with $\overline{Mv} = 0$ at the inner bank and $\overline{Mv} = \bar{M}_+\delta$ at the outer bank gives

$$(W\langle H\overline{Mu}\rangle)_x = -W\langle M(-b)w_s(-b)\rangle - \bar{M}_+\delta - \int_{r_0 - W/2}^{r_0 + W/2} \frac{H\overline{Mv}}{r}\, dr \tag{A7}$$

For narrow channels the integral is small compared to $\bar{M}_+\delta$, so

$$(W\langle H\overline{Mu}\rangle)_x = -W\langle M(-b)w_s(-b)\rangle - \bar{M}_+\delta \tag{A8}$$

Equations (A8) and (A4) have the same form as their counterparts (9) and (10), and these latter equations are recovered exactly, except for the settling velocity w_s appearing instead of the effective sedimentation velocity w_s, if H, M, and u are vertically and laterally uniform as was assumed. What is lost by making this assumption has now been made explicit. By taking $\langle H\bar{u}\rangle = \langle H\rangle\langle\bar{u}\rangle$ and $\langle H\overline{Mu}\rangle = \langle H\rangle\langle\bar{M}\rangle\langle\bar{u}\rangle$ we have ignored terms which involve the downstream divergence of the products of the differences of these quantities from their mean values. This is a necessary penalty in the absence of more detailed observations but one which is appropriate for the order of magnitude estimates which are sought here.

Equation (A8) has been derived by making the implicit assumption that M, u, v, and w represent time-averaged values. If instead we were to replace these quantities in (A5) by $M + \tilde{m}$, $u + \tilde{u}$, $v + \tilde{v}$ and $w + \tilde{w}$, where the tildes denote turbulent fluctuations, and then average with respect to time, Reynolds flux terms would appear. These take the form $(\tilde{m}\tilde{u})_x$, $(\tilde{m}\tilde{v})_r$, $\tilde{m}\tilde{v}/r$, and $(\tilde{m}\tilde{w})_z$, where the time average is understood. It is reasonable to assume that the axial and transverse scales of the turbulence are large in comparison to the vertical length scales, the latter being of the same order as the bottom and interfacial boundary layer thicknesses. Only the $(\tilde{m}\tilde{w})_z$ term is retained therefore. When integrated in the vertical, this gives $-\tilde{m}\tilde{w}$ at the bottom ($z = -b$), since there can be no mean flux of sediment across the upper interface in the steady state. The effective sedimentation velocity can now be written in the form

$$Mw_s = M(-b)w_s(-b) - \tilde{m}\tilde{w}(-b) \tag{A9}$$

This would replace the term in angle brackets in (A8). Since M

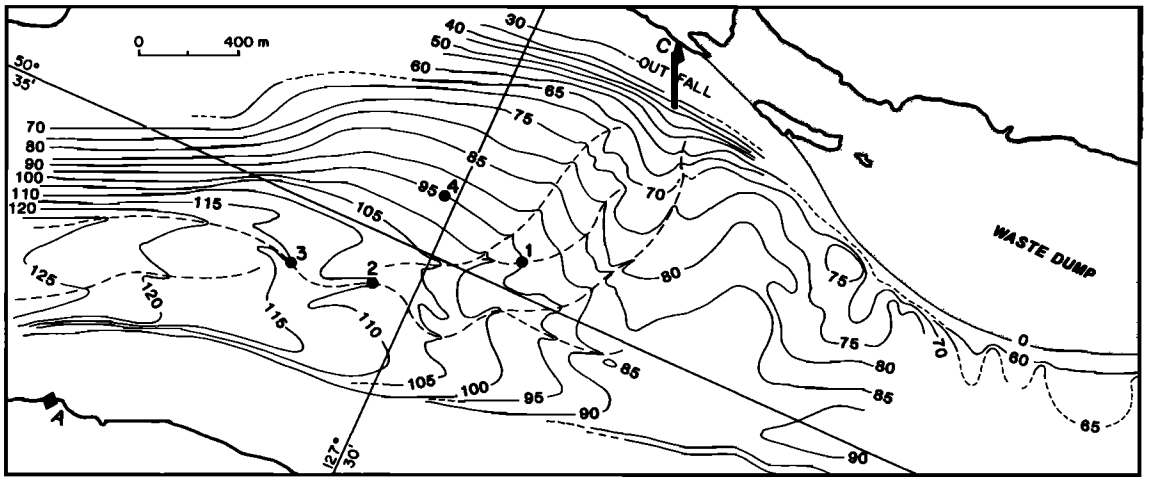

Fig. A1. Apron phase. Tailing deposit bathymetry in September 1978. Contours in meters. Anchor station locations are shown as solid circles.

increases toward the bed, $\tilde{m}\tilde{w}$ is expected to be positive at the bed, and hence $w_s < w_*$ as stated earlier.

The momentum balance can be handled similarly. Consider the steady form of the Navier-Stokes equations in cylindrical coordinates. The downstream component is

$$uu_x + vu_r + wu_z + \frac{uv}{r} - fv = \xi gM \sin\beta + \frac{1}{\rho_0}\frac{\partial \tau}{\partial z} \qquad \text{(A10)}$$

Because lateral scales are taken to be large, only the vertical gradient of the shear stress is included. After integrating in the vertical as before this becomes

$$(\overline{Hu^2})_x + (\overline{Huv})_r + \frac{\overline{Huv}}{r} - Hf\bar{v} = \xi gH\bar{M} \sin\beta + \frac{\tau_0 + \tau_i}{\rho_0} \qquad \text{(A11)}$$

where it has been assumed that ambient fluid entrained at the interface has no momentum. *Smith and McLean* [1984] have derived a similar equation for flow in a river bend. For (A11) to take the same form as (8) we must assume that $\overline{Hu^2} \sim H\bar{u}\,\bar{u}$ and $\overline{uv} \sim \bar{u}\,\bar{v}$ and make use of (A1). Doing so gives

$$H\bar{u}\,\bar{u}_x + H\bar{v}\,\bar{u}_r - Hf\bar{v} = \xi gH\bar{M} \sin\beta - \bar{u}w_e + \frac{\tau_0 + \tau_i}{\rho_0} \qquad \text{(A12)}$$

which is the same form as (8) except for the term in w_s, which does not appear because sedimentation has been ignored here, and those in $\bar{v}$. The cross-stream velocity was assumed to be vanishingly small compared to $\bar{u}$ in section 5, and if this is done in (A12), the form of (8) is recovered.

It should be noted that *Dietrich and Smith* [1983] have shown that the terms $(\overline{Hu^2})_x$, $(\overline{Huv})_r$, and $\overline{Huv}/r$ in (A11) are important in laboratory subaereal channels and in a river meander. However, $0.27 \leq W/r_0 \leq 0.5$ in these channels, which were therefore not narrow in the sense used here. Furthermore, they were in equilibrium with the mean flow, which we have decided was probably not the case in Rupert Inlet.

APPENDIX 2: TIDAL CURRENTS AND INLET CIRCULATION

Tidal currents could be important in the context of this study in two respects: They might exert a net influence on the behavior of the discharge plume, and they might cause significant transport of tailing out of the proximal zone. Rupert Inlet is part of a tidally energetic system exhibiting pronounced seasonal variations associated with an annual deep water exchange cycle [*Drinkwater and Osborn*, 1975; *Stucchi and Farmer*, 1976; *Stucchi*, 1985].

The only current measurements in the area of interest off the mine site are those reported by *Johnson* [1974] and *Hay* [1981], the latter of whom discussed both sets of measurements at length. Briefly summarizing, the near-bottom currents at depths of about 100 m or more are semidiurnal, are aligned roughly parallel to the inlet axis, and often exhibit a net down-inlet drift when integrated over a tidal cycle. The down-inlet drift is not always present and varies in amplitude over the fortnightly tidal cycle. Variations also occur on seasonal time scales as a function of the deep water exchange cycle, but these are not as well documented. In *Hay*'s [1981] results at least part of the down-inlet motion is almost certainly due to the downslope flow of the discharge plume. *Johnson* [1974] however, presents a near-bottom current meter record acquired on the southern flank of the inlet (between A and Hankin Point in Figure 1) at a depth of 108 m, some 45 m shallower than the inlet floor. Because of the depth these data would not be expected to have been affected by the discharge plume and indicate a mean down-inlet speed which is at times as large as 10 cm s^{-1}. The amplitude of the time-varying tidal signal was about 30 cm s^{-1}, so that the instantaneous current, tidal plus mean, can be 40 cm s^{-1}, which is quite large. *Hay* [1981] reported measurements of near-bottom currents made from a moored ship farther up-inlet during the apron phase at stations 1–4 (Figure A1). These data indicate a similar pattern: 30 cm s^{-1} tidal amplitudes with a mean down-inlet drift near 10 cm s^{-1}. The down-inlet speeds increased toward the bottom, and part of this net down-inlet motion was therefore attributed to the discharge plume. Because of this and because the inlet narrows considerably to the west where Johnson's measurements were made, the contribution from the inlet circulation is taken to be 5 cm s^{-1}. This choice is also supported by the fact that velocities tended to decrease headward and shoreward of stations 2 and 3, that is, toward stations 1 and 4 (Figure A1).

There are unfortunately no current measurements available for one of the areas of greatest interest, which is the area off the outfall where the upper reach was located. One of the best indications that we have of the effects of tidal currents on the discharge plume in this reach is therefore the set of acoustic images discussed previously, and exemplified by Figure 4. Nevertheless, an estimate of the importance of the net drag

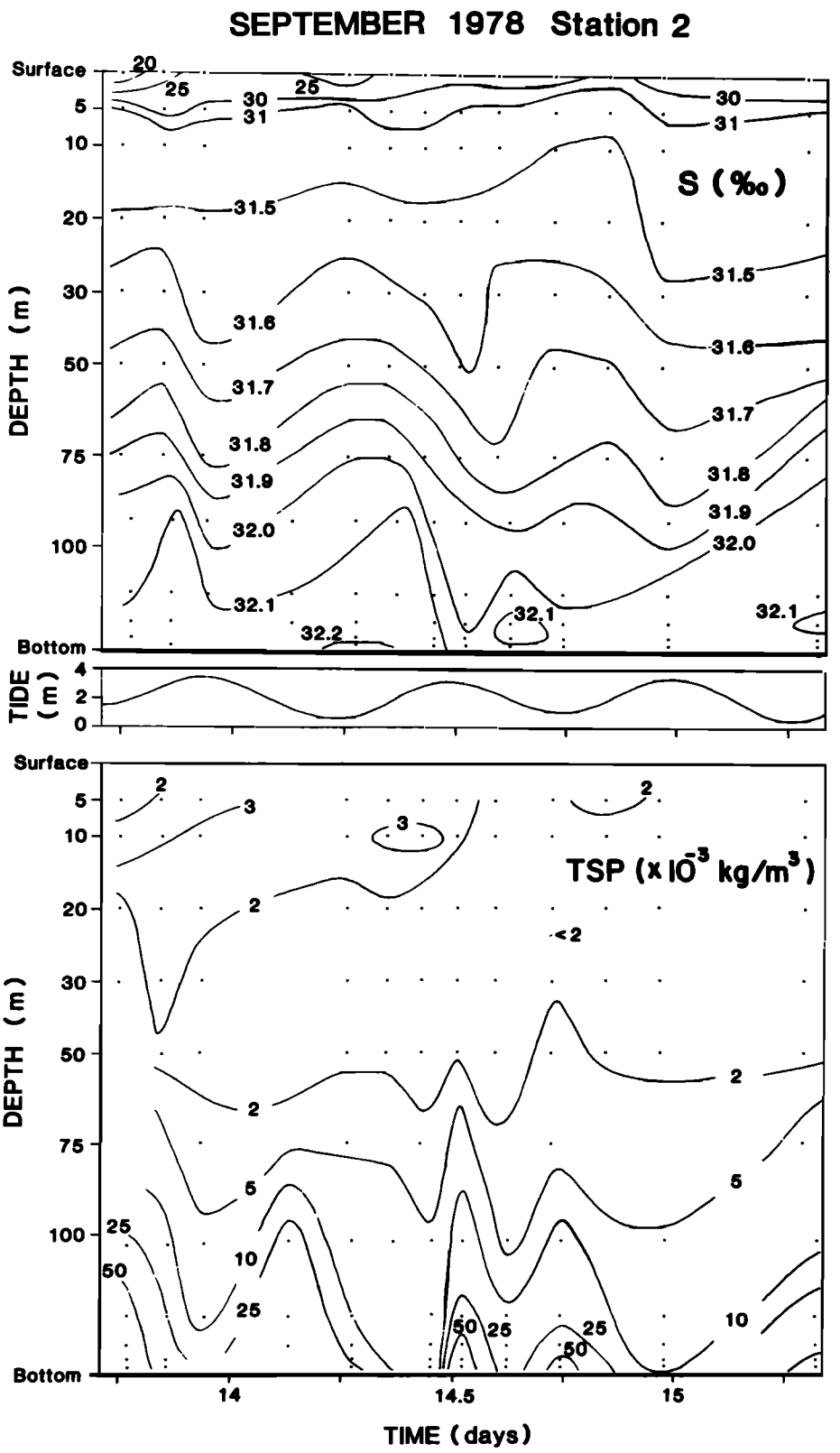

Fig. A2. Apron phase. Time series of total suspended particulate (TSP, in units of 10^{-3} kg m^{-3}), predicted tidal height, and salinity in September 1978 at station 2 (Figure A1). Bottom depth = 116 m.

exerted by tidally induced currents on the discharge plume can be made. These currents, which will be called ambient currents to distinguish them from the density current generated by the discharge, are assumed to be directed perpendicular to the upper reach. They are designated by $v_a = v(t) + v$, where $v(t) = v_0 \sin \omega t$ represents the semidiurnal tidal current and v is the down-inlet drift. We let the instantaneous drag on the turbidity current interface exerted by the ambient currents

be given by

$$\frac{\tau_a}{\rho_0} = C_i v_a^2 \tag{A13}$$

where C_i is a drag coefficient. In time-averaged form this becomes, for $v_0 \gg v$, $\tau_a/\rho_0 = 8C_i v_0 v/\pi$. The appropriate dynamical comparison is between this interfacial stress and the cross-channel pressure gradient in the vertically integrated form of (1). That is,

$$\sigma = \frac{\tau_a/\rho}{\xi g M H\, \Delta h/W} = \frac{8C_i v_0 v}{\pi \xi g M H\, \Delta h/W} \tag{A14}$$

It remains to estimate the value of the interfacial drag coefficient C_i. One approach, which has the merit of being consistent with the results obtained earlier, is to use a value for C_i estimated from the overall drag coefficient f'' determined for the turbidity current. First, we define a bottom drag coefficient C_D such that $\tau_0/\rho_0 = C_D u^2$ and let $C_i u^2$ represent the sum of the interfacial stress τ_i/ρ_0 and entrainment. The relation between f'', C_D, and C_i is therefore

$$\frac{f''}{2} = C_D + C_i \tag{A15}$$

We are interested in the maximum possible value of σ and therefore of C_i. Examining (A15), we see that this corresponds to choosing the maximum possible value of f'' and the minimum possible value of the bottom drag coefficient C_D. Because side scan records show that the channel banks are rough [*Hay et al.*, 1983*a*; *Hay*, 1981], the value of C_D is set equal to 2.6×10^{-3}, which corresponds to the average of the smallest values found by *Sternberg* [1986] for indistinctly roughened sand. Setting $f'' = 0.013$, we obtain $C_i = 4 \times 10^{-3}$. With $v_0 =$ 30 cm/s, $v = 5$ cm/s, $\Delta h/W = 3.5/62$, $M = 0.25$ kg m^{-3}, and $H = 8$ m, we obtain 0.2 as the maximum possible value for σ. This suggests that the net stress on the discharge plume was probably a second order effect.

In order to evaluate the probable transport out of the proximal zone by the down-inlet drift, consider the time series of suspended solids concentrations in Figure A2. These measurements were made at station 2 (Figure A1). Concentrations rise above background levels in the zone between 75-m depth and the bottom (116 m). The time- and depth-averaged concentration in this zone is 0.015 kg m^{-3}. The average depth of the zone is 95 m, and the width of the inlet at station 2 at this depth is about 920 m (Figure A1). From this width the average concentration above, a down-inlet drift of 5 cm/s, and a 50-m thickness for the high-concentration zone, a transport rate of about 30 kg/s is obtained. This is about the same as the transport rate estimated for continuous turbidity flow.

The above arguments lead to the conclusion that tidal currents and the induced inlet circulation are unlikely to have either induced a net interfacial stress on the discharge plume comparable to the transverse pressure gradient or to have been the primary mechanism for transport of material out of the proximal zone. Further, there is reason to believe that the estimates of these effects are themselves excessive. *Johnson* [1974] reported, for example, that although the maximum speeds over a tidal cycle were usually down-inlet, the largest near-bottom currents were, in fact, up-inlet and occurred in conjunction with the waning spring tide. These periods of high up-inlet currents were not taken into account in the above analysis and would reduce the estimates. In addition, the current measurements referred to above were made during the summer and early fall, a period of low runoff when water carried into the inlet over the sill during the latter stage of the flood tide is more dense than the near-surface waters in the inlet. This incoming water penetrates to middepth and at times to the bottom, inducing the large currents observed at depth [e.g., *Stucchi and Farmer*, 1976; *Stucchi*, 1985]. During the late fall and winter, runoff associated with rainfall becomes mixed with the water carried into the inlet by the tide, and penetration to depth does not occur, resulting in more quiescent near-bottom conditions. It is noteworthy that the acoustic images like that in Figure 4 were acquired during such a period in late November 1976, and current speeds measured at 80-m depth at this time were small: 7 cm/s maximum [*Hay*, 1981]. This also suggests that the annual average net tidal stress and transport rate would be smaller than estimated above.

Acknowledgments. I thank my thesis supervisors, R. W. Burling and J. W. Murray and the technical staff at the University of British Columbia, where the field work was carried out. R. Hiscott, R. W. Burling, and Y.-H. Jin made useful comments on an earlier version of this manuscript. The study was supported by strategic grant G0208 and grant A8446 from the Natural Sciences and Engineering Research Council, Canada. Newfoundland Institute for Cold Ocean Science contribution 120.

REFERENCES

Bagnold, R. A., Autosuspension of transported sediments: Turbidity currents, *Proc. R. Soc. London, Ser. A.*, *265*, 315–319, 1962.

Batchelor, G. K., *An Introduction to Fluid Dynamics*, 615 pp., Cambridge University Press, New York, 1967.

Bellaiche, G., V. Coutellier, L. Droz and P. Masson, Deep-sea and Martian channels, *Deep Sea Res.*, *33*, 973–980, 1986.

Bo Pedersen, F., *A Monograph on Turbulent Entrainment and Friction in Two-Layer Stratified Flow.*, 397 pp., Institute of Hydrodynamics and Hydraulic Engineering, Technical University of Denmark, Lyngby, 1980*a*.

Bo Pedersen, F., Dense bottom currents in rotating ocean, *J. Hydraul. Div. Am. Soc., Civ. Eng.*, *106*(HY8), 1291–1308, 1980*b*.

Bowen, A. J., W. R. Normark and D. J. W. Piper, Modelling of turbidity currents on Navy submarine fan, California borderland, *Sedimentology*, *31*, 169–185, 1984.

Carstens, T., and E. Tesaker, Erosion by artificial suspension current, paper presented at 13th Coastal Engineering Conference, Am. Soc. of Civ. Eng., Vancouver, B. C., 1972.

Damuth, J. E., V. Kolla, R. D. Flood, R. O. Kowsmann, M. C. Monteiro, M. A. Gorini, J. J. C. Palma, and R. H. Belderson, Distributary channel meandering and bifurcation patterns on the Amazon deep-sea fan as revealed by long-range side-scan sonar (GLORIA), *Geology*, *11*, 94–98, 1983.

Dietrich, W. E., and J. D. Smith, Influence of the point bar on flow through curved channels, *Water Resour. Res.*, *19*, 1173–1192, 1983.

Drinkwater, K. F., and T. R. Osborn, The role of tidal mixing in Rupert and Holberg inlets, *Limnol. Oceanogr.*, *20*, 518–529, 1975.

Hay, A. E., Submarine channel formation and acoustic remote sensing of suspended sediments and turbidity currents in Rupert Inlet, B. C., Ph.D. thesis, 326 pp., Univ. of B. C. Vancouver, 1981.

Hay, A. E., On the remote acoustic detection of suspended sediment at long wavelengths, *J. Geophys. Res.*, *88*, 7525–7542, 1983.

Hay, A. E., Turbidity currents and submarine channel formation in Rupert Inlet, British Columbia, 1, Surge observations, *J. Geophys. Res.*, this issue.

Hay, A. E., and R. Waters, A diatom chronology for sediments in a high accumulation rate environment: Rupert Inlet, British Columbia, *Limnol. Oceanogr.*, *30*, 898–906, 1985.

Hay, A. E., R. W. Burling, and J. W. Murray, Remote acoustic detection of a turbidity current surge, *Science*, *217*(4562), 833–835, 1982.

Hay, A. E., J. W. Murray, and R. W. Burling, Submarine channels in Rupert Inlet, British Columbia, I, Morphology, *Sediment. Geol.*, *36*, 289–315, 1983*a*.

Hay, A. E., J. W. Murray, and R. W. Burling, Submarine channels in

Rupert Inlet, British Columbia, 2, Sediments and sedimentary structures, *Sediment. Geol.*, *36*, 317–339, 1983*b*.

Johnson, R. A., Dispersal of recent sediments and mine tailing in a shallow-silled fiord, Rupert Inlet, British Columbia, Ph.D. thesis, 181 pp., Univ. of B. C., Vancouver, 1974.

Komar, P. D., The channelized flow of turbidity currents with application to the Monterey deep sea fan channel, *J. Geophys. Res.*, *74*, 4544–4558, 1969.

Komar, P. D., Continuity of turbidity current flow and systematic variation in deep-sea channel morphology, *Geol. Soc. Am. Bull.*, *84*, 3329–3338, 1973.

Komar, P. D., Computer simulation of turbidity current flow and the study of deep-sea channels and fan sedimentation, in *The Sea*, vol. 6, edited by E. D. Goldberg, I. N. McCave, J. J. O'Brien, and J. H. Steele, pp. 603–622, John Wiley, New York, 1977.

Menard, H. W., Deep-sea channels, topography and sedimentation, *Am. Assoc. Pet. Geol. Bull.*, *40*, 2195–2210, 1955.

Normark, W. R., and F. H. Dickson, Man-made turbidity currents in Lake Superior. *Sedimentology*, *23*, 815–831, 1976*a*.

Normark, W. R., and F. H. Dickson, Sublacustrine morphology in Lake Superior, *Am. Assoc. Pet. Geol. Bull.*, *60*, 1021–1036, 1976*b*.

Piper, D. J. W., and W. R. Normark, Turbidite depositional patterns and flow characteristics, Navy submarine fan, California borderland, *Sedimentology*, *30*, 681–694, 1983.

Smith, J. D., and S. R. McLean, A model for flow in meandering streams, *Water Resour. Res.*, *20*, 1301–1315, 1984.

Sternberg, R. W., Friction factors in tidal channels with differing bed roughness, *Mar. Geol.*, *6*, 243–260, 1968.

Stucchi, D. J., The tidal jet in Rupert Inlet, *Atmos. Ocean*, *23*, 118–136, 1985.

Stucchi, D. J., and D. M. Farmer, Deep water exchange in Rupert-Holberg Inlet, *Pac. Mar. Sci. Rep. 76-10*, 32 pp., Inst. of Ocean Sci., Patricia Bay, Sydney, B. C., Canada, 1976.

Tesaker, E., Modelling of suspension currents, in *Symposum on Modeling Techniques*, pp. 1385–1401, American Society of Civil Engineers, New York, 1975.

A. E. Hay, Department of Physics and Newfoundland Institute for Cold Ocean Science, Memorial University of Newfoundland, St. John's, Newfoundland, Canada A1B 3X7.

(Received April 15, 1986;
accepted August 26, 1986.)